研究論文

Crystallographic Texture Formation of Pure Tantalum by Selective Laser Melting Method

Jongyeong OH*, Takuya ISHIMOTO*, Shi-hai SUN*,** and Takayoshi NAKANO*

（Received May 5, 2019）

Selective laser melting（SLM）is a type of additive manufacturing（AM）process that can produce functional parts with complicated 3-D structures from various types of metals. Recent studies have revealed that SLM can be a potential tool not only for shape control, but also for control of the crystallographic texture of metallic materials. Texture control of refractory metals and biomaterials is an important strategy to improve their functionality. Modern SLM devices are capable of high output and can melt refractory metals that generally exhibit high melting points. In this study, we undertook the fabrication of tantalum, a typical refractory metal, through SLM and investigated its crystallographic texture formation. Tantalum parts that were nearly completely dense with a relative density of more than 99 vol.% and specific crystal orientation of <111> fiber- like texture along the building direction were developed.

Key Words: Selective Laser Melting（SLM）, Tantalum, Refractory Materials, Biomaterials, Crystallographic Texture

1. Introduction

Additive manufacturing（AM）has attracted considerable attention as an advanced technology that enables the fabrication of parts of various shapes. The control of crystallographic texture formation in metal parts has recently become an important topic in metal AM technology[1)-7)] as it has an impact on anisotropy in mechanical properties such as Young's modulus and yield stress. These advantageous features are being applied in a variety of fields, especially in the military, medical, and aerospace industries[8)-11)].

Fig. 1 shows a schematic illustration of the powder bed fusion-type AM process. First, 3-D modeling is conducted for the target design of the desired shape determined by using computer-aided design（CAD）. The 3-D shaped pattern is then sliced into 2-D units. The process parameters such as scan speed, beam power, pitch, and layer thickness are adjusted and appropriate conditions are set for the shape and material of the target parts. The fabrication commences after setting all the process parameters and consists of repeating the process of selective melting and solidifying one layer at a time.

Selective laser melting（SLM）is a novel powder bed fusion-type AM process for manufacturing parts with high precision and geometric freedom. A laser beam is used as the heat source to fabricate 3-D complex shapes. Recently, it has received significant attention as the energy density of laser beams is high enough to melt refractory metal powder such as tantalum（Ta）[12),13)].

Ta is a rare metal that belongs to the elemental group 5A and exists in a body-centered cubic equilibrium phase（α-Ta）and the metastable tetragonal（β-Ta）phase. It exhibits high density（16.69 g/cm^3）, high melting point（2996℃）, good resistance to oxidation, and superior biocompatibility[14)]. Owing to these characteristics, it is used in a variety of fields such as aerospace, biomedical, and electronic devices[15)]. However, there are many restrictions in its applications owing to its high price and difficulties in the manufacturing process. Post-processing at high working operation temperature and protection from oxidation are required in the standard manufacturing process of Ta and Ta-

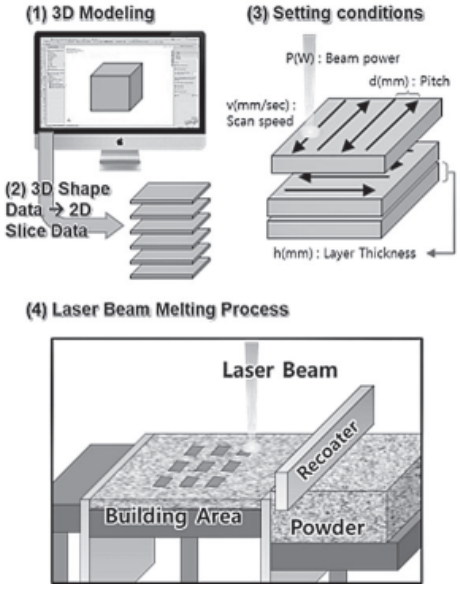

Fig. 1 Schematic image of selective laser melting process.

＊大阪大学大学院工学研究科マテリアル生産科学専攻（565-0871 大阪府吹田市山田丘 2-1）
Division of Materials and Manufacturing Science, Graduate School of Engineering, Osaka University（2-1, Yamadaoka, Suita, Osaka 565-0871, Japan）
＊＊大阪大学異方性カスタム設計・AM 研究開発センター（565-0871 大阪府吹田市山田丘 2-1）
Anisotropic Design & Additive Manufacturing Research Center, Osaka University（2-1, Yamadaoka, Suita, Osaka 565-0871, Japan）

alloys[16]. However, in the SLM process it is possible to reduce the consumption of materials and control the crystallographic texture formation, which cannot be accomplished in the standard manufacturing process. For instance, it is important for the crystallographic texture of Ta to be anisotropically controlled in medical devices for bone fracture fixation as the anisotropic bone functions are dominantly controlled by the anisotropic arrangement of collagen fibers and apatite crystals as a bone quality index[17)-28)].

In this study, pure Ta parts were fabricated by the SLM process to investigate the crystallographic texture formation.

2. Experimental details

Flake-shaped Ta powder was obtained from H. C. Starck（Germany）for the fabrication of pure Ta specimens. The powder exhibited an irregular morphology（**Fig. 2**）and had a particle size of less than 45 μm.

The SLM process was conducted using an M 290 AM machine（EOS, Germany）in a high purity argon atmosphere containing not more than 90 ppm of oxygen gas. Specimens with dimensions of 10 × 10 × 10 mm were fabricated under bidirectional（zigzag）laser scanning along the x-axis（Scan Strategy X）. The x-axis, y-axis, and z-axis were assigned as the scanning direction（SD）, transverse direction（TD）and building direction（BD）, respectively.

The relative density was measured using Archimedes' method. The sample was cut by electric discharge machining along the y-z plane（**Fig. 3**）. The specimen was polished with SiC sandpaper and buffed for two hours using a colloidal silica solution. The buffed specimens were etched in a solution comprising 10 ml of HF, 10 ml of HNO_3, 30 ml of H_2SO_4, and 50 ml of H_2O. The constituent phase and crystallographic orientation were analyzed using an X-ray diffractometer（X' pert PRO, Philips, Netherlands）with Cu Kα radiation operating at 45 kV and 40 mA. The diffraction data were taken in a 2θ range from 30° to 120° at a step size and scan rate of 0.001° and 1°/min, respectively. The microstructure and crystallographic orientation distributions were analyzed by field emission scanning electron microscopy（FE-SEM, JSM-6500F, JEOL, Japan）and electron backscatter diffraction（EBSD, Symmetry, Oxford Instruments, UK）.

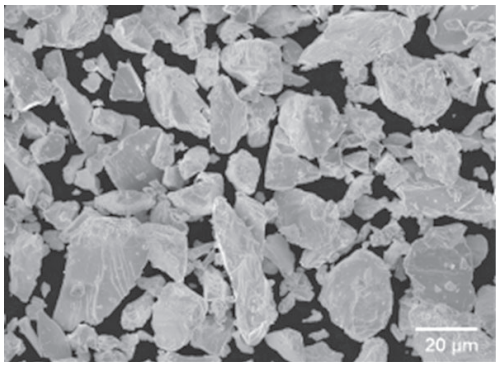

Fig. 2 FE-SEM image of pure Ta powder

3. Results and discussion

Fig. 3 shows the image of the manufactured products. The production of some specimens stopped prematurely as collisions with the recoater occurred during the process. **Fig. 4** shows the optical microscope image in the plane perpendicular to the SD, TD, and BD of a typical specimen. An almost completely dense body with a relative density of 99.3% was obtained; obvious large porosities or cracks were not observed in the specimen comprising plate-like elements parallel to the scanning direction（SD）and building direction（BD）stacked in the transverse direction（TD）.

Fig. 5 shows the X-ray diffraction patterns of Ta powder and the SLM-fabricated specimen along SD and BD. All the peak positions are identical and correspond to those of the standard pattern for pure Ta with a body-centered cubic structure[29] in which the diffraction peaks appear at 2θ of 38.47° for（110）, 55.55° for（200）, 69.58° for（211）, 82.46° for（220）, 94.94° for（310）, and 107.64° for（222）. A peak of Ta oxide, such as Ta_2O_5, was not detected owing to the protection against oxidation via argon replacement during the SLM process. The relative peak intensity in the SLM-fabricated specimen differed from that in the powder material, indicating an evolution of prominent preferential crystallographic orientation within the specimen. {111} preferentially aligns in the BD, while {110} strongly appears in

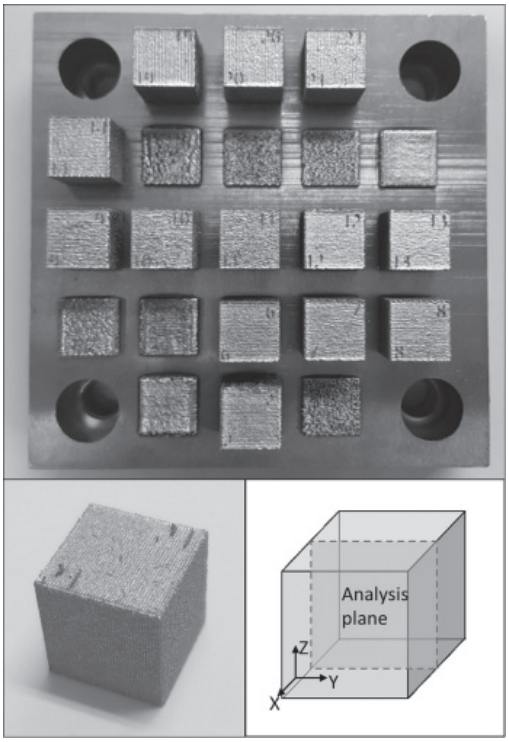

Fig. 3 Captured image of the pure Ta specimen on the substrate plate after SLM process.

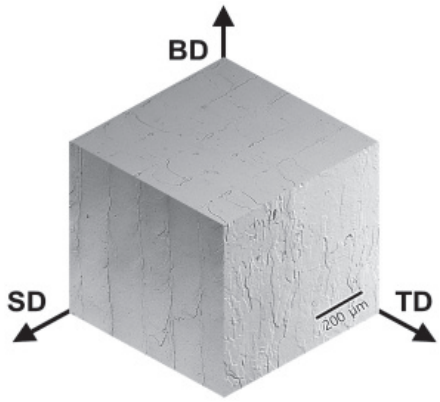

Fig. 4 Optical microscope image of pure Ta specimen.

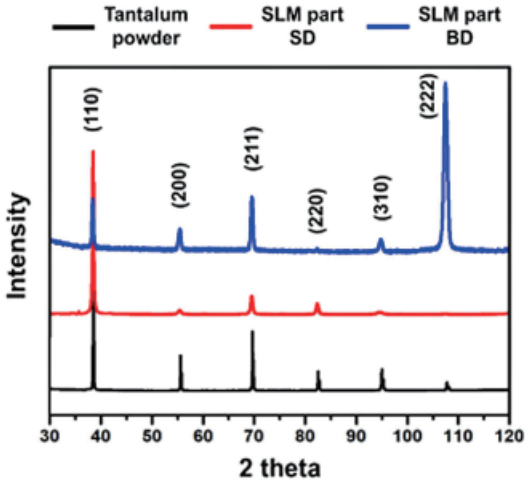

Fig. 5 X-ray diffraction patterns of Ta powder and SLM parts on the surface perpendicular to the scanning direction (SD) and building direction (BD).

the SD.

The crystallographic orientation was also determined by inverse pole figure (IPF) maps (**Fig. 6**) and the corresponding pole figures (**Fig. 7**) acquired in the y-z plane (i.e., the cross section perpendicular to the SD) of the specimen. In the IPF maps, a columnar (cross-section of plate-like elements) microstructure was observed. In a single column, the crystallographic orientation tended to be inherited through the layers, which indicates that an epitaxial growth occurred in the BD (z-axis). Consequently, a fiber texture-like orientation distribution was formed, in which <111> strongly orients in the BD. However, the orientation around <111> was not uniform; an orientation distribution with a faint three-fold symmetry was observed (**Fig. 7**). The texture formation with three-fold symmetry is somewhat strange as geometric factors that induce three-fold symmetry were not included in the fabrication condition. Our previous studies using Ti-, Ni- and Fe-based alloys, with cubic crystallographic symmetry[1),4)-7)] in which <100> was an easy growth direction with maximum thermal gradient[30)] and a single crystalline-like texture, rather than a

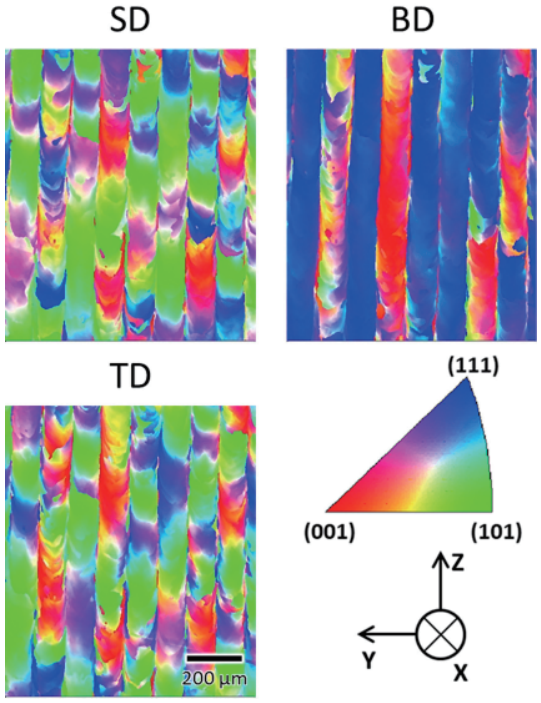

Fig. 6 Inverse pole figure maps representing crystallographic orientation distribution along x-, y-, and z-axes.

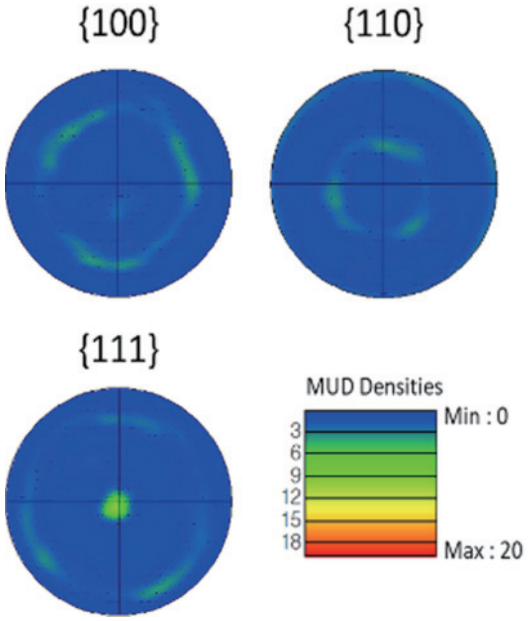

Fig. 7 Pole figures generated based on Fig. 6.

fiber-type, evolved where <110> preferentially orients in the BD under the Scan Strategy X. This texture was derived by a two-directional growth of the cell parallel to <100> elongated along ±45° from the BD in the y–z plane in the melt pools[1)]. For Ta, the ±45° cellular growth did not occur. Similar <111> orientation along the BD was reported in SLM-fabricated parts of W-alloy[31)] which is another typical refractory metal.

The SLM is a unique process in which solidification behavior

in a small melt pool dominates the texture[6]. As the solidification behavior occurs at high speed in a limited region and therefore cannot be observed *in situ*, it is difficult to understand the overall phenomena of texture evolution. Various thermophysicochemical properties such as specific heat, thermal conductivity, and diffusion coefficient of solid and liquid phases affect the melt pool shape and solidification behavior in the melt pool. The largely different thermophysicochemical properties between（Ta and W）and（Ti, Ni, and Fe）may affect the melt pool shape and resultant migration direction of the solid–liquid interface, leading to varied crystallographic texture. The elucidation of the mechanism for crystallographic texture formation requires further studies combining microstructure observation and computer simulation. Further study is currently in progress and will be reported later.

4. Conclusion

In this study, Ta parts with high relative density were fabricated using the SLM method under the Scan Strategy X. A fiber-like texture with prominent <111> orientation in the BD evolved in the specimen, which was quite different from the texture formation in Ti-, Ni-, and Fe-based alloys.

Acknowledgments

This work was supported by the Grants-in-Aid for Scientific Research（S）（JP18H05254）from the Japan Society for the Promotion of Science（JSPS）, Cross-Ministerial Strategic Innovation Promotion Program（SIP）, Material revolution by material integration（Development of 3-D additive manufacturing process of Ni-based alloy）from Japan Science and Technology Agency（JST）.

References

1） T. Ishimoto, K. Hagihara, K. Hisamoto, S.H. Sun and T. Nakano: Scripta Mater., **132**（2017）34-38.
2） K. Hagihara, T. Nakano, M. Suzuki, T. Ishimoto, Suyalatu, S.H. Sun and T. Ishimoto: J. Alloys Compd., **695**（2017）67-72.
3） M. Todai, T. Nakano, T. Liu, H. Y. Yasuda, K. Hagihara, K. Cho, M. Ueda and M. Takeyama: Addit. Manufact., **13C**（2017）61-70.
4） S.H. Sun, K. Hagihara and T. Nakano: Mater. Des., **140**（2018）307-316.
5） T. Ishimoto, J. Yasutomi, S, Sugimoto, T. Nakano: Journal of Smart Processing, **7**（2018）229-232.
6） S.H. Sun, T. Ishimoto, K. Hagihara, Y. Tsutsumi, T. Hanawa and T. Nakano: Scripta Mater., **159**（2019）89-93.
7） T. Nagase, T. Hori, M. Todai, S.H. Sun and T. Nakano: Materials & Design, **173**（2019）Paper# 107771.
8） T. Nagase, M. Todai, T. Hori and T. Nakano: J. Alloys Compd.,**753**（2018）412-421.
9） M. Todai, T. Nagase, T. Hori, A. Matsugaki, A. Sekita and T. Nakano: Scripta Mater., **129C**（2017）65-68.
10） K. Hagihara, Y. Hama, K. Yuge and T. Nakano: Acta Mater., **61**（2013）3432-3444.
11） T. Nakano, Y. Nakai, S. Maeda and Y. Umakoshi: Acta Mater., **50**（2002）1781-1795.
12） L. Thijs, M.L. M. Sistiaga, R. Wauthle, Q. Xie, J.P. Kruth and J.Van Humbeeck: Acta Mater., **61**（2013）4657-4668.
13） L. Zhou, T. Yuana, R. Li, J. Tang, G. Wang and K. Guo: Mater. Sci. Eng. A, **707**（2017）443-451.
14） A. Al-Masha'Al, A. Bunting and R. Cheung: Appl. Surf. Sci., **371**（2016）571-575.
15） C. Sungail and A. Abid: Metal Powder Rep., **73**（2018）316-318.
16） K.D. Moser: JOM, **51**（1999）29-31.
17） T. Nakano and T. Ishimoto: KONA Powder and Particle J., **32**（2015）75-84.
18） T. Nakano, K. Kaibara, Y. Tabata, N. Nagata, S. Enomoto, E. Marukawa and Y. Umakoshi: Bone, **31**（2002）479-487.
19） T. Ishimoto, T. Nakano, M. Yamamoto and Y. Tabata: J. Mater. Sci. Mater. Med., **22**（2011）969-976.
20） T. Nakano, K. Kaibara, T. Ishimoto, Y. Tabata and Y. Umakoshi: Bone, **51**（2012）741-747.
21） A. Matsugaki, G, Aramoto and T. Nakano: Biomaterials, **33**（2012）7327-7335.
22） T. Ishimoto, T. Nakano. Y. Umakoshi, M. Yamamoto and Y. Tabata: J. Bone Miner. Res., **28**（2013）1170-1179.
23） A. Matsugaki, N. Fujiwara and T. Nakano: Acta Biomater., **9**（2013）7227-7235.
24） Y. Noyama, T. Nakano, T. Ishimoto, T. Sakai and H. Yoshikawa: Bone, **52**（2013）659-667.
25） A. Matsugaki, G. Aramoto, T. Ninomiya, H. Sawada, S. Hata and T. Nakano: Biomaterials, **37**（2015）134-143.
26） T. Ishimoto, B. Sato, J.W. Lee and T. Nakano: Bone, **103**（2017）216-223.
27） Y. Kimura, A. Matsugaki, A. Sekita and T. Nakano: Sci. Rep., **7**（2017）paper#44824.
28） R. Ozasa, T. Ishimoto, S. Miyabe, J. Hashimoto, M. Hirao, H. Yoshikawa and T. Nakano: Calcif. Tissue Int., **104**（2019）449-460.
29） JCPDS-ICDD card file 04-0788.
30） R.W. Messler: Principles of Welding, Wiley, NY（2008）.
31） C. Tan, K. Zhou, W. Ma, B. Attard, P. Zhang and T. Kuang: Sci. Technol. Adv. Mater., **19**（2018）370-380.

Mail Address
ishimoto@mat.eng.osaka-u.ac.jp